

Investigation on Electromagnetic Shielding System of Indoor Air-Core Reactor Using Multi-Parameter Variable Optimization

Hongping XIE^a and Zhe CHEN^{a,1}

^aState Grid Jiangsu Electric Power Co. Ltd Construction Branch, Nanjing 210036, China

Abstract. In order to solve the problem of serious electromagnetic pollution and metal equipment heating around the indoor air-core reactor due to its magnetic leakage, this paper adopts the ANSYS finite element simulation platform to carry out three-dimensional electromagnetic modeling of the indoor air-core reactor and its surrounding facilities and the house structure of the 500kV substation, and installs shielding plates on the top of the house. By optimizing and analyzing multi-parameter variables such as the material, thickness, and gap width of the shielding body, a system was developed to improve the electromagnetic environment around the indoor reactor. Simulation results show that: in the steel beam above the installation of 3mm thickness aluminum plate overlap into the shielding plate, can effectively reduce the magnetic induction intensity of the steel structure of the house. Temperature variation of the reactor during operation meets the insulation heat resistance class required for air-core reactor. The temperature of the edge section of the shielding device is high, the maximum point is 53.26°C, and the average temperature of the surrounding building facilities rises by about 5~10°C, which satisfies the standards for safe operation.

Keywords. Air-core reactor, finite element simulation, shielding, magnetic induction intensity, temperature field

1. Introduction

In recent years, power grid system develops rapidly. In order to cope with the demand for large-capacity and high-load power consumption, reactor, as one of the common reactive power compensation devices, plays an increasingly important role in the power grid [1,2]. The dry-type air-core reactor has excellent characteristics such as strong shock resistance, good linear characteristics, low loss, low noise, simple structure, etc., which is of great significance for the improvement of power quality in indoor substations [3].

However, as people's safety awareness increases, the electromagnetic pollution generated by air-core reactors has become a common concern for the environmental protection industry and the power industry. Compared with outdoor substations, the equipment in indoor sites is more compact, and the electric field distortion will be intensified during operation, which may lead to corona discharge or even breakdown,

¹ Zhe CHEN, Corresponding author, State Grid Jiangsu Electric Power Co. Ltd Construction Branch, Nanjing 210036, China; E-mail: jerryji0127@gmail.com.

and it is very easy to cause a rapid rise in ambient temperature, threatening the safe operation of electrical equipment [4].

Researches found that the installation of low resistivity material shielding structure can provide some shielding effect. But the device is not convenient for the operation and maintenance of electrical equipment [5]. It is also possible to use the shielding structure of high permeability materials, but it will lead to a higher shielding plate flux, and the system is easy to overheating [6]. In addition, the use of distributed air gap design instead of the traditional method of opening a centralized air gap can also effectively reduce the leakage inductance and the eddy current loss generated by the magnetic lines passing through the windings. However, it is needed to change the internal structure of the reactor and is not conducive to a wide range of applications.

Therefore, this paper proposes an optimization scheme of electromagnetic shielding device for air-core reactor taking into account the economy and reliability for the problem of high temperature of steel beam above the reactor caused by high magnetic field. Based on the multi-parameter optimization method, electromagnetic shielding devices with different materials, sizes, and lap-jointed forms were designed and installed above the steel beams, solving the problem of inconvenient installation or maintenance of the reactor while protecting the house structure more precisely. At the same time, ANSYS Maxwell three-dimensional finite element simulation software was used to model the indoor air-core reactor and its surrounding facilities and housing structure [8]. The shielding performance was comprehensively compared based on the multi-field simulation results of the magnetic field and the temperature field, and the optimal scheme was selected and verified.

2. Analysis of Losses in Air-core Reactors

The ANSYS simulation software used in this paper is based on the finite element method and applies the variational principle and subdivision idea to divide the air-core reactor into non-overlapping sets of units, thus simplifying the process of analyzing and solving the electromagnetic field [7].

When using ANSYS to carry out temperature field simulations, it is necessary to provide it with loss data for the components in the substation. The total resistance loss that it produces is calculated by summing the resistance losses of the n -layer coils:

$$P_R = \sum_{i=1}^n I_i^2 R_i \quad (1)$$

where I_i and R_i are the current and resistance of the coil in layer i , respectively.

Meanwhile, under the influence of the alternating magnetic field and resistance, the air-core reactor also generates circulating current loss P_h and eddy current loss P_E in each layer of coil during operation:

$$P_h = \sum_{i=1}^n \left[I_i^2 R_i - \left(\frac{I}{n} \right)^2 R_i \right] \quad (2)$$

$$P_E = \sum_{i=1}^n \sum_{j=1}^{m_i} \frac{\pi^2 d_i^4 \gamma \omega^2}{32} r_i B^2 \quad (3)$$

where I is the total encapsulation current, m_i , d_i and r_i are the number of turns, radius and wire diameter of the layer i , respectively.

3. Modeling and Simulation of Indoor Substation

After being put into operation, Suzhou Yuexi 500kV substation found that the strong magnetic field generated by the air-core reactor interfered with the surrounding electrical equipment, and there was heat generation in the steel structure and flooring, which seriously affected the reliability and safety of the equipment operation. Also, there was a large potential hazard for occupational exposure. This paper carries out simulation analysis for the arrangement scheme of the substation, including a 66kV reactor of model ZJKK-280-10 and two sets of 35kV three-phase reactors of model CKJKL-2400/35-12, as well as the surrounding equipment brackets and steel buildings, etc. The analysis maximizes the scenario of the substation layout. The parameters of the three-phase reactors, which are highlighted in the discussion, are shown in table 1.

Table 1. Reactor Model Parameters.

| Reactor Model | CKJKL-2400/35-12 |
|---|------------------|
| Phase Number | Three-phase |
| Rated Voltage/kV | 35 |
| Rated Current/A | 833.3 |
| Encapsulation Layer Number | 2 |
| Encapsulation Layer Height/mm | 1302 |
| Air Flue Width/mm | 150 |
| Encapsulation Layer Width/mm | 25 |
| Min Inner Diameter of Encapsulation Layer/mm | 1450 |
| Max Inner Diameter of Encapsulation Layer /mm | 1840 |
| Overall Height/mm | 5092 |

In order to appropriately speed up the simulation, the following assumptions can be made in the modeling process:

(1) Some cylindrical parts such as equipment brackets, encapsulation, surge arresters and ground switches are replaced by dodecagonal columns;

(2) Define the winding current density per unit length uniformly distributed and ignore the influence of eddy currents between windings on the magnetic field distribution;

(3) Simplify each layer of encapsulations into a cylinder with a certain thickness and ignore the external insulating layer of encapsulation;

(4) The brace between the encapsulations of the air-core reactor and some small connectors basically do not affect the magnetic field distribution, so they are ignored in the modeling.

A 1:1 model is built according to the actual scene of this indoor substation, including reactors, ground switches, surge arresters, shunt capacitors, current transformers, and steel beams and columns of the house, etc. Then, materials corresponding to each part are selected to obtain the model as shown in figure 1.

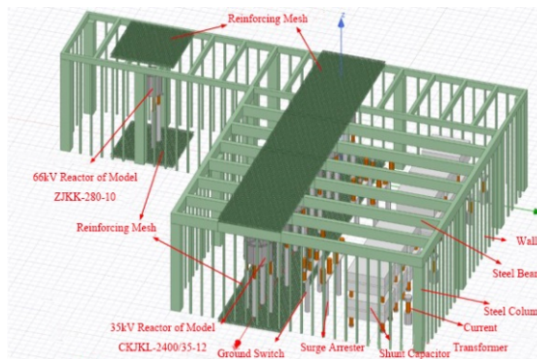


Figure 1. Simulation Model of Indoor Substation.

After the modeling is completed, the solution domain, excitation and boundary conditions are set, and the mesh generation density is checked [9]. Also, the magnetic field distribution around the reactor is obtained through data processing after the simulation is completed, so as to carry out further analyses and provide loss data for the temperature field simulation.

The following assumptions are made on the surrounding environment in the temperature field simulation:

(1) The indoor ambient temperature is set to 40°C, and the radiant temperature between the indoor air-core reactor encapsulation layers and with other electrical equipment are all 40°C;

(2) Set the indoor wind speed to 1.5 m/s. The fluid domain on the left side of the reactor is the inlet boundary and the right side is the outlet boundary; the relative pressure is zero.

According to the heat source parameters of the reactor obtained by electromagnetic simulation after installing the shielding device, the overall model is imported into the 'Icepak' module of the ANSYS Work-bench platform. The boundary conditions and basic parameters are set according to the indoor working conditions, and the mesh is performed according to the physical model. Specific implementation steps are as follows:

(1) Set parameters such as calculation area, wall data, boundary conditions, etc. in Cabinet;

(2) Set material properties and heat source data for CAD Object components in the geometry model in Blocks;

(3) Set the mesh cell type, mesh size and other parameters of the geometric model, and install 'Assembly' to refine the mesh size of the reactor body and shielding device. Then, check the mesh quality after mesh generation;

(4) Set the parameters of 'Solver' solver and use iteratively solving. Then, process to obtain the maximum temperature and average temperature distribution of the indoor air-core reactor model.

4. Magnetic Field Simulation and Result Analysis

In order to better explore the influence of the magnetic field around the reactor on the house structure, this paper carries out accurate modeling for one group of three-phase reactors and their surrounding house structure. The dimensions of the house structure are shown in table 2 and the model is shown in figure 2. Wherein, the current excitation within each envelope of the three phases of the reactor A, B, and C is set to $80 \angle 0^\circ \text{kA}$, $80 \angle 120^\circ \text{kA}$, and $80 \angle -120^\circ \text{kA}$ respectively.

Table 2. Model Dimensions of the Building Structure.

| House Structure | Specific Dimensions/mm |
|-----------------------------------|--|
| Length, width and height of house | 113000×4000×6900 |
| Reinforcing Mesh | Bi-directional reinforcing mesh with 12 diameters and 100 spacing |
| Steel Column | H-pipe in size 600×600×20×20, height 6200 |
| Stud Wall | 100×100 square steel pipes with 600 horizontal and 1200 vertical spacing |
| Steel Beam | H-pipe in size HN700×300×13×2, 2000 spacing |
| Steel Plate | Pressurized steel plates with the thickness of 1.6 |

While keeping the structure of the house and the layout of the equipment unchanged, the electromagnetic exceeding and heating problem of the indoor three-phase reactor can generally be mitigated by installing a shielding structure. Installing it between the steel beams and plates does not affect the connection and maintenance access of the reactor to the surrounding electrical equipment, and at the same time better shields the electromagnetic radiation to the house structure. In the following section, the material and thickness of the shielding structure, as well as the width of the gap during layout, will be used to select a shielding solution with optimal performance in all aspects.

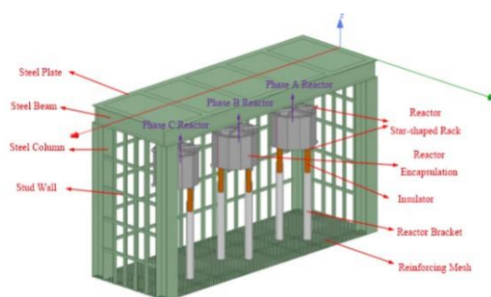


Figure 2. Three-phase Reactor and its Surrounding Building Structure Model.

4.1. Analysis of the Influence of Material Properties on the Shielding Effect

In order to compare the shielding effect of metal plates of different materials, common shielding materials iron, aluminum and copper were selected to produce shielding plates with a thickness of 3 mm, which were placed above the steel beams. Among them, iron belongs to the high permeability material, which provides a path for the magnetic field, limiting the spread of magnetic lines of force and reducing the leakage

field. Aluminum and copper are high electrical conductivity materials, which produce induced currents in the conductor when the magnetic field changes, generating a magnetic field in the opposite direction to counteract the original magnetic field.

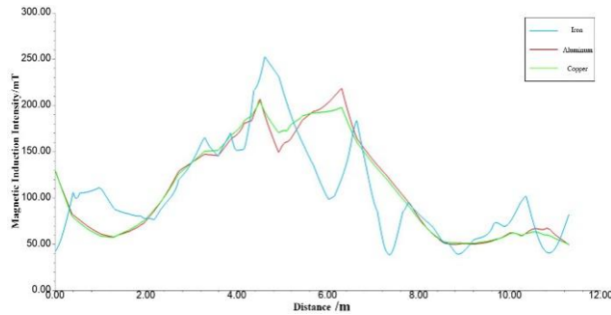


Figure 3. Magnetic Induction Intensity of Steel Plate with Different Material Shielding Plate.

As can be seen in figure 3, the shielding effect of aluminum and copper plates is similar, while the magnetic induction intensity on the steel plate fluctuates greatly when using iron plates, reaching 251.85 mT at the highest point. Magnetic field simulations were performed to obtain the losses incurred by the steel plates when using these three different materials for shielding, and the temperature field was used to calculate the maximum temperatures of the shield itself and the steel plate above it in the same environment. Also find information to get the price per square meter of 3mm thickness of iron, aluminum and copper plates, as shown in table 3.

Table 3. Simulation Temperature and Price of Different Material Shielding Plate.

| Shielding Plate Material | Iron | Aluminum | Copper |
|--|--------|----------|---------|
| Steel Plate Loss/W | 445.64 | 210.584 | 210.629 |
| Max Temperature of Steel Plate /°C | 54.175 | 53.366 | 54.721 |
| Max Temperature of Shielding Plate /°C | 54.201 | 53.372 | 54.757 |
| Price/RMB/m ³ | 750 | 300 | 800 |

According to table 3, it is found that when these three materials are selected as shielding plates, the temperatures of themselves and the steel plates are similar, with a difference of only 1.385°C at most. However, the use of aluminum shielding temperature is relatively low, and its loss is only 47.31% of the iron plate, while the price of aluminum plate is much lower than iron and copper plate. Considering the shielding effect, loss, temperature and price, the shielding plate whose material is aluminum is finally selected as the research object.

4.2. Analysis of the Effect of Lap Gap Width on Shielding Effect

Shielding plates are often laid in lots of small sized plates spliced together, resulting in some gaps between the smaller plates. The existence of this gap causes the magnetic field to partially leak to the steel beam, resulting in partial high magnetic field and reduced shielding effectiveness. The magnetic field intensity H_g through the gap in the shielding plate is

$$H_g = H_0 e^{-\frac{\pi t}{g}} \tag{4}$$

where H_0 is the original magnetic field below the shielding plate; t and g are the thickness of the shielding plate and the gap width, respectively. So, when t is determined and when g is smaller, H_g is also smaller and the shielding effect is better.

In the simulation, it is assumed that the shielding plate is all composed of small aluminum plates of $1m \times 1m$ of 3mm thickness, and the aluminum plates with gap widths of 0mm, 5mm, and 10mm are selected to verify the influence of the gap width of the shielding plate on the shielding effect.

The magnetic induction intensity at six points on the upper surface of the steel plate as shown in figure 4 were collected separately for the unshielded device and for different gap widths of the aluminum plate. The collected data are shown in table 4.

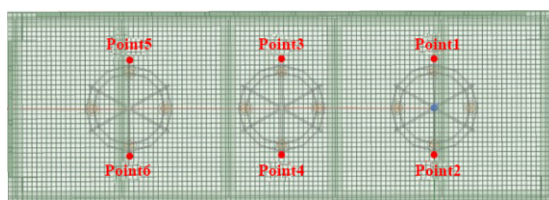


Figure 4. Position of 6 Points on the Upper Surface of Steel Plate.

From table 4, it can be seen that the installation of shielding device can effectively reduce the magnetic field intensity on the steel plate, and the smaller the gap, the less the magnetic leakage, which is consistent with the expression of equation (7); When the gap is 0mm, the average value of magnetic induction intensity at 6 points decreases to 44.21% of that without shielding device. Therefore, when laying the shielding plate in the project, each aluminum plate should be connected by overlapping laps to shorten the gap width to zero.

Table 4. The Magnetic Induction Intensity Values at the Positions of 6 Points under Different Conditions.

| Point Position | Magnetic Induction Intensity at 0mm gap /T | Magnetic Induction Intensity at 5mm gap /T | Magnetic Induction Intensity at 10mm gap /T | Magnetic Induction Intensity without shielding /T |
|----------------|--|--|---|---|
| Point 1 | 0.13685 | 0.16671 | 0.14794 | 0.45639 |
| Point 2 | 0.26840 | 0.23934 | 0.26762 | 0.72452 |
| Point 3 | 0.23073 | 0.27815 | 0.32369 | 0.68263 |
| Point 4 | 0.39724 | 0.35191 | 0.42642 | 0.73851 |
| Point 5 | 0.15486 | 0.18017 | 0.17018 | 0.34602 |
| Point 6 | 0.27268 | 0.35428 | 0.30754 | 0.35569 |
| Average Value | 0.24346 | 0.26176 | 0.27390 | 0.55063 |

4.3. Analysis of the Effect of Shielding Plate Thickness on Shielding Effect

According to Eq. (4), theoretically, when the thickness t of the shielding material is larger, the H_g will be smaller and the shielding effect is more obvious, but the cost and the difficulty of installation will increase. In order to compare the effect of shielding plate thickness on the shielding effect, three control groups were set up with gap width

of 0mm, 5mm and 10mm. After a series of simulations, the magnetic induction intensity curve on the line where the x-axis direction is located at 7m from the ground, i.e., 10cm above steel beam, is obtained as shown in figure 5.

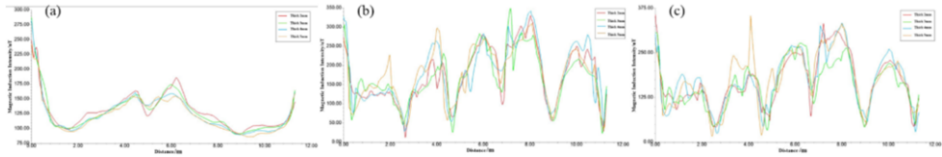


Figure 5. Magnetic Induction Intensity of Steel Plate when Using (a) 0mm, (b) 5mm, (c) 10mm Thicknesses of Shielding Plate.

Observing the three sets of curves in figure 5, it is found that the magnetic induction intensity curves are relatively flat at the gap width of 0 mm, with an overall slight decrease with increasing thickness, but the difference is small; When there is a lap gap width, the fluctuation of the magnetic induction intensity curve corresponding to each thickness of the shielding plate increases and lacks regularity. For this reason, it is necessary to further analyze the temperature field simulation to obtain the maximum temperature of the steel plate in each case as shown in table 5.

Table 5. Temperature of Steel Plate under Different Conditions.

| Plate Thickness/mm | Gap Width/mm | | |
|--------------------|--------------|--------|--------|
| | 0 | 5 | 10 |
| 2 | 54.1°C | 51.4°C | 55.8°C |
| 3 | 53.2°C | 52.6°C | 53.5°C |
| 4 | 53.3°C | 53.8°C | 53.7°C |
| 5 | 52.7°C | 52.9°C | 54.1°C |

As can be seen from table 5, when the thickness of the shielded aluminum plate is 3 mm, the average temperature of the steel plate is lower, and the magnetic leakage at this time is also relatively less. According to figure 5, the gap width of the shielding plate has less influence on the magnetic field, but when the aluminum plate is thicker, the cost and weight will be higher, also the application in the project will be more complicated, so thinner shielding plate is a perfect choice. Meanwhile, considering the temperature rise, it was determined that an aluminum plate with a gap width of 0 mm and a thickness of 3 mm was selected as the shielding plate.

5. Magnetic and Temperature Field Simulation Verification

Further verification and analysis of the electromagnetic and temperature environment of the reactor group and its surroundings will carry out after installation of shielding plates.

5.1. Magnetic Field Simulation Verification

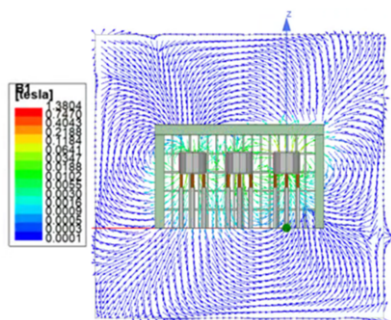


Figure 6. Diagram of Section Magnetic Force of Reactor Stack.

Through the magnetic field simulation, the diagram of section magnetic force of the reactor, and magnetic field distribution of the house structure are obtained, as shown in figures 6 and 7, respectively.

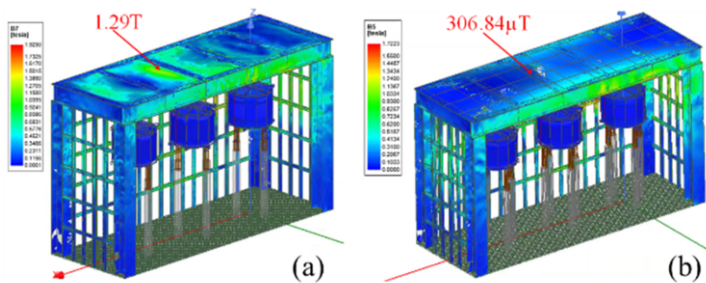


Figure 7. Magnetic Field Distribution of Reactor Group and Building Structure (a) Before, (b) After Installing Shielding Device.

Without shielding equipment, the highest magnetic induction intensity on the upper surface of the steel plate in the x-axis direction on the median axis is 1.29 T. After the installation of the shielding plate, the value is reduced to 306.84 μ T, which shows that the program effectively mitigates the electromagnetic exceedance problem of the housing environment.

5.2. Temperature Field Simulation Verification

In the ‘Icepak’ module, the loss values calculated from the electromagnetic simulation before and after the installation of the shielding plate are applied to the indoor air-core reactor model using Eq. (5) as a heat source excitation, respectively.

$$P = P_R + P_E \tag{5}$$

The thermal analysis calculation is completed iteratively by setting the parameters such as calculation area, boundary conditions, material properties, and precision mesh generation, solver settings, etc. The post-processing results can be obtained as the

temperature distributions of the reactor and the house model, and the temperature values of the main components are labeled in the figure, as shown in figure 8.

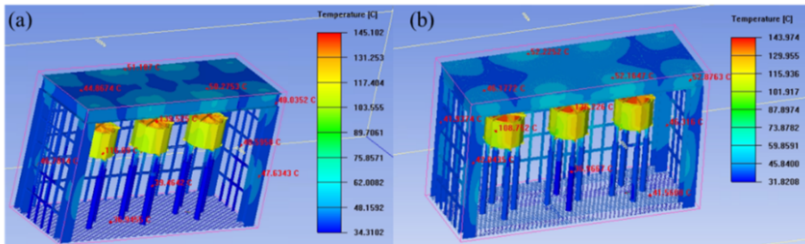


Figure 8. Magnetic Field Distribution of Reactor Group and Building Structure (a) Before, (b) After Installing Shielding Device.

The reactor temperature data obtained from the simulation are similar to the simulated reactor temperature in references [2] and [10], which verifies the feasibility and accuracy of the simulation method. Comparing the temperature field cloud diagrams of the reactor group and the distribution of temperature values of each component before and after the installation of shielding devices, it is found that the temperature of the reactor body and the building facilities such as steel plates, steel beams and steel columns are reduced after the installation compared with that before the installation, and the temperature values of the main components are shown in the table 6 below.

Table 6. Temperature Comparison of Main Components before and after Installing Shielding Device.

| Facilities | Before Installing | | After Installing | |
|--------------|-------------------|--------------|------------------|--------------|
| | Max Temp./°C | Avg Temp./°C | Max Temp./°C | Avg Temp./°C |
| Reactor Body | 145.10 | 119.03 | 143.97 | 114.94 |
| Steel Column | 52.00 | 44.90 | 51.37 | 44.85 |
| Steel Beam | 61.98 | 49.01 | 61.75 | 48.83 |
| Steel Plate | 55.77 | 47.72 | 53.26 | 45.81 |

The temperature of the reactor body (phase A) and the surrounding stud walls (taking the wall with the highest temperature), steel beams, steel columns (taking the steel column with the highest temperature), and ground reinforcing mesh and other facilities after the installation of shielding devices are specifically shown in the table 7 below:

Table 7. Temperature Value of Reactor Body and Surrounding Building Materials.

| Facility | Loss/W | Max Temp./°C | Avg Temp./°C |
|--------------------------|---------|--------------|--------------|
| Outer Encapsulation | 9678.65 | 132.73 | 112.41 |
| Inner Encapsulation | 8038.77 | 143.97 | 133.40 |
| Upper Star-shaped Rack | 1141.74 | 138.84 | 131.96 |
| Lower Star-shaped Rack | 1232.08 | 132.11 | 124.31 |
| Reactor Insulators | / | 87.15 | 50.03 |
| Reactor Bracket | / | 41.73 | 38.58 |
| Shielding Aluminum Plate | 391.26 | 53.26 | 45.18 |
| Stud Wall | 735.52 | 60.73 | 46.47 |
| Steel Beam | 586.27 | 61.75 | 48.83 |
| Steel Plate | 208.0 | 53.26 | 45.81 |
| Steel Column | 25.93 | 51.37 | 44.85 |
| Reinforcing Mesh | 100.89 | 42.15 | 38.83 |

After comparing the encapsulation layers of the reactor body, it was found that temperature of encapsulation located in the inner layer is higher than that of the outer, which is due to outer encapsulation directly exchanging heat with the outside world, and the heat is fully convected [10]. The highest point temperature of the model simulation is 143.973°C, which satisfies the turn-to-turn insulation heat resistance class H and the overall insulation heat resistance class F for this type of dry type air core reactor. The shielding plate is selected to observe its temperature distribution.

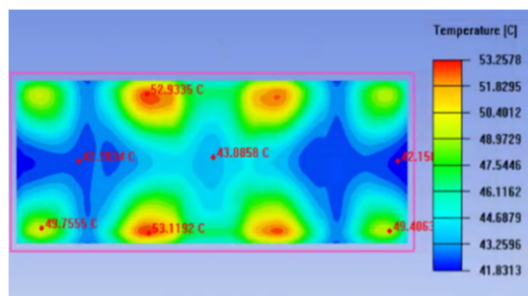


Figure 9. Cloud Image of Temp. Distribution of Shielding Plate.

It can be seen from figure 9 that the highest value of the temperature of the shielding aluminum plate is 53.26°C, which is located at the edge of the shielding structure, and the rest of the locations have lower temperatures, with an average temperature of 45.18°C.

It was found that the temperature would rise more in the part of the two reactor gap, and the hot air exchanged with the outside world at the top and bottom of the reactor encapsulation would have a certain rise on the temperature of the steel bracket. Overall, the average temperature of the surrounding building facilities increases by about 5 to 10°C compared to the room temperature, so the operation of the indoor air-core reactor has little effect on it.

6. Conclusion

For the indoor air-core reactor leakage problem, a realistic 3D model was constructed, and an optimized solution to build a shielding plate above it was proposed, combining multiple parameter factors such as material, thickness and gap width. The accuracy of the model is verified by electromagnetic field and temperature field simulation, which is a good reference value for future design and operation of indoor substations and the improvement of electromagnetic environment of air-core reactor. Key points are as follows:

(1) When an aluminum shielding plate is used, the house steel plate produces small losses, has a low operating temperature, and the aluminum plate is relatively inexpensive for this model scenario;

(2) By collecting the magnetic induction intensity on the upper surface of the steel plate, it was found that the smaller the width of the gap between the shielding plates, the better the electromagnetic shielding effect, so aluminum plates should be overlapped;

(3) Comparing the magnetic field and temperature around the steel plate at different thicknesses, it is found that the shielding plate of 3mm thickness is effective, has low temperature, and is lightweight, low cost, and suitable for reactor shielding scenarios;

(4) Verification of aluminum shielding plates installations overlapped by 3mm thickness above the steel beams found that the magnetic leakage on the steel plates was significantly reduced, and the average temperature of the surrounding building facilities increased by only 5~10°C compared with the room temperature to satisfy the reactor insulation level and indoor safe operation conditions.

Acknowledgments

This work is supported by Science and Technology Project of State Grid Jiangsu Electric Power Co., LTD (J2021098).

References

- [1] Wang YH, Meng ZH, Song YX. Analysis of influencing factors on site fault diagnosis of inter-turn short circuit fault of dry-type air-core shunt reactor. 2018 12th International Conference on the Properties and Applications of Dielectric Materials (ICPADM), Xi'an, China. 2018 Jul; pp. 713-716.
- [2] Dong JX, Shu NQ, Yan QQ, et al. Coupling calculation and analysis of temperature field of dry-type air-core shunt reactor during overheat fault. *Engineering Journal of Wuhan University*. 2018 May;51(05): 437-442.
- [3] Ping Dy, Ge JB, Hao WG, et al. Air-core reactor common operating problems and treatment. *Electric Age*. 2020 Jan;(09):45-46.
- [4] Cui ZG, Qian GC, Yang L, et al. Study on electromagnetic shielding of the distributed current sensor for dry-type air-core reactor. 2020 IEEE International Conference on High Voltage Engineering and Application (ICHVE), Beijing, China. 2020 Dec; pp. 1-4.
- [5] Li N, Zhang M, Feng JX, et al. Research on magnetic field shielding of air-core reactor based on finite element method. *Electric Power Survey & Design*. 2020 Mar;(03):32-36.
- [6] Wu Q. Magnetic shielding research of air-core reactor based on Ansoft. *Journal of Electrical Engineering*. 2019 Jun;14(02):61-65.
- [7] Gu L, Liu XG, He J, et al. Analysis of strand-to-strand short circuit magnetic field of dry hollow reactor unit based on ANSYS. *Computer Simulation*. 2019 Sep;36(09):103-108.
- [8] Jiang W, Jia ZH. Research of the magnetic field distribution of 35kV Dry-Type Air-Core parallel reactor based on finite element method. *Power & Energy*. 2020 Aug;41(04):421-424.
- [9] Ye GH, Lv LX, Hong L. Effect of Grounding Defect on High-voltage XLPE Cable Terminal. *Electric Power Engineering Technology*. 2018 Jul; 37(04):137-142.
- [10] Wu SY, Ma HZ, Jiang N, et al. Simulation and analysis of temperature field of high voltage reactor based on multi physical field coupling. *Power System Protection and Control*. 2019 Feb; 47(04):17-24.